

Multi-Robot Object SLAM using Distributed Variational Inference

Hanwen Cao

Sriram Shreedharan

Nikolay Atanasov

Abstract—Multi-robot simultaneous localization and mapping (SLAM) enables a robot team to achieve coordinated tasks relying on a common map. However, centralized processing of robot observations is undesirable because it creates a single point of failure and requires pre-existing infrastructure and significant multi-hop communication throughput. This paper formulates multi-robot object SLAM as a variational inference problem over a communication graph. We impose a consensus constraint on the objects maintained by different nodes to ensure agreement on a common map. To solve the problem, we develop a distributed mirror descent algorithm with a regularization term enforcing consensus. Using Gaussian distributions in the algorithm, we derive a distributed multi-state constraint Kalman filter (MSCKF) for multi-robot object SLAM. Experiments on real and simulated data show that our method improves the trajectory and object estimates, compared to individual-robot SLAM, while achieving better scaling to large robot teams, compared to centralized multi-robot SLAM. Code is available at https://github.com/intrepidChw/distributed_msckf.

I. INTRODUCTION

Simultaneous localization and mapping (SLAM) [1] is a fundamental problem for enabling mobile robot to operate autonomously in unknown unstructured environments. In robotics applications, such as transportation, warehouse automation, and environmental monitoring, a team of collaborating robots can be more efficient than a single robot. However, effective coordination in robot teams requires a common frame of reference and a common understanding of the environment [2]. Traditionally, these requirements have been approached by relying on a central server or lead robot [3], [4], which communicates with other robots to receive sensor measurements and update the locations and map for the team. However, communication with a central server requires pre-existing infrastructure, introduces delays or potential estimation inconsistency, e.g., if the server loses track of synchronous data streams, and creates a single point of failure in the robot team. Hence, developing distributed techniques for multi-robot SLAM is an important and active research direction. A fully decentralized SLAM system enables robots to communicate opportunistically with connected peers in an ad-hoc network, removing the need for multi-hop communication protocols and centralized computation infrastructure. It allows flexible addition or removal of robots in the team and, by extending the scalability of the algorithm, enables coverage of larger areas with improved localization and map accuracy.

We gratefully acknowledge support from NSF FRR CAREER 2045945 and ARL DCIST CRA W911NF-17-2-0181.

The authors are with the Department of Electrical and Computer Engineering, University of California San Diego, La Jolla, CA 92093, USA, e-mails: {h1cao, sshreedharan, natanasov}@ucsd.edu.

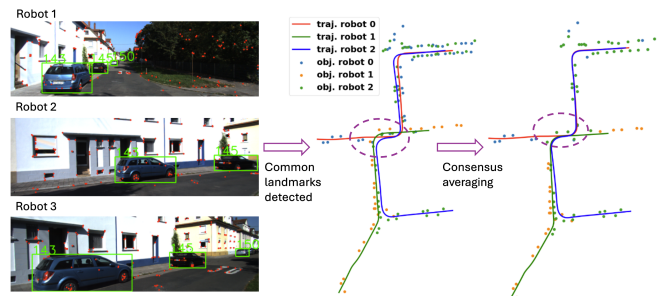


Fig. 1: Illustration of multi-robot object SLAM via distributed multi-state constraint Kalman filtering. The left images are inputs for the robots, where the red are geometric features (extracted by FAST [5]) and the green are object detections (by YOLOv6 [6]). The geometric features and object bounding box centroids are used as observations. When common objects are observed by communicating robots, a consensus averaging step is performed to align the estimated robot trajectories and object positions.

This paper considers a multi-robot landmark-based SLAM problem. We develop an approach for distributed Bayesian inference over a graph by formulating a mirror descent algorithm [7] in the space of probability density functions and introducing a regularization term that couples the estimates of neighboring nodes. Our formulation allows joint optimization of common variables (e.g., common landmarks among the robots) and local optimization of others (e.g., private robot trajectories). As a result, each node is able to keep a distribution only over its variables of interest, enabling both efficient storage and communication. By using Gaussian distributions in the mirror descent algorithm, we derive a distributed version of the widely used multi-state constraint Kalman filter (MSCKF) [8] with an additional averaging step to enforce consensus for the common variables. We apply the distributed MSCKF algorithm to collaborative object SLAM using only stereo cameras at each robot. In the prediction step, each robot estimates its trajectory locally using visual odometry. In the update step, the robots correct their trajectory estimates using both visual features and object detections. As is common in the MSCKF, we avoid keeping visual landmarks in the robot states using a null-space projection step. However, object landmarks are kept as a map representation at each robot and are shared among the robots during the consensus averaging step to collaboratively estimate consistent object maps. In short, each robot estimates its pose trajectory and an object map locally but communicates with its neighbors to reach agreement on the object map across the robots.

The contributions of this work are summarized as follows.

- We formulate multi-robot landmark SLAM as a varia-

tional inference problem over a communication graph with a consensus constraint on the landmark variables.

- We develop a distributed mirror descent algorithm with a regularization term that couples the marginal densities of neighboring nodes.
- Using mirror descent with Gaussian distributions, we obtain a distributed version of the MSCKF algorithm.
- We demonstrate multi-robot object SLAM using stereo camera measurements for odometry and object detection on both real and simulated data to show that our method improves the overall accuracy of the trajectories and object maps of robot teams, compared to individual-robot SLAM, while achieving better scaling to large robot teams, compared to centralized multi-robot SLAM.

II. RELATED WORK

SLAM is a broad research area including a variety of estimation methods [8]–[10] as discussed in [1], [11]–[14]. Performing SLAM with multiple collaborating robots improves efficiency but also introduces challenges related to distributed storage, computation, and communication. This section reviews recent progress in multi-robot SLAM.

A. Multi-robot pose graph optimization

Tian et al. [15] propose a certifiably correct pose graph optimization (PGO) method with a novel Riemannian block coordinate descent (RBCD) that can operate in a distributed setting. Considering both localization and mapping, Cunningham et al. [16], [17] extend Smoothing and Mapping (SAM) [18] by introducing a Constrained Factor Graph that enforces consistent estimations of common landmarks among robots. Choudhary et al. [19] developed a two-stage approach using Successive Over-Relaxation and Jacobi Over-Relaxation to split the computation among the robots. MR-iSAM2 [20] extends incremental smoothing and mapping (iSAM2) [10] by introducing a novel data structure called mult-root Bayes tree. Tian et al. [21] investigate the relations between Hessians of Riemannian optimization and Laplacians of weighted graphs and propose a communication-efficient multi-robot optimization algorithm with a central server performing approximate second-order optimization.

Recent SLAM systems utilize the theoretical results of the above works to achieve efficient multi-robot operation. Kimera-Multi [22], a fully distributed dense metric-semantic SLAM system, uses a two-stage optimization method built upon graduated non-convexity [23] and RBCD [15]. DOOR-SLAM [24] uses [19] as a back-end and pairwise consistency maximization [25] for identifying consistent measurements across robots. Xu et al. [26] develop a distributed visual-inertial SLAM combining collaborative visual-inertial odometry with an alternating direction method of multipliers (ADMM) algorithm and asynchronous distributed pose graph optimization [27]. Andersson et al. [3] design a multi-robot SLAM system built upon square-root SAM [18] by utilizing rendezvous-measurements.

B. Multi-robot filtering

Roumeliotis and Bekey [28] showed that the Kalman filter equations can be written in decentralized form, allowing decomposition into smaller communicating filters at each robot. Thrun et. al [29] presented a sparse extended information filter for multi-robot SLAM, which actively removes information to ensure sparseness at the cost of approximation. With nonlinear motion and observation models, a decentralized extended Kalman filter (EKF) has an observable subspace of higher dimension than the actual nonlinear system and generates unjustified covariance reduction [30]. Huang et al. introduced observability constraints in EKF [30] and unscented smoothing [31] algorithms to ensure consistent estimation. Gao et al. [32] use random finite sets to represent landmarks at each robot and maintain a probability hypothesis density (PHD). The authors prove that geometric averaging of the robot PHDs over one-hop neighbors leads to convergence of the PHDs to a global Kullback-Leibler average, ensuring consistent maps across the robots. Zhu et al. [33] propose a distributed visual-inertial cooperative localization algorithm by leveraging covariance intersection to compensate for unknown correlations among the robots and deal with loop-closure constraints.

Compared to existing work, our contribution is to derive a fully distributed filtering-based system for landmark-based SLAM from a constrained variational inference perspective. Our formulation makes a novel connection to distributed mirror descent and enables robots to achieve landmark consensus efficiently with one-hop communication only and without sharing private trajectory information.

III. PROBLEM STATEMENT

Consider n robots seeking to collaboratively construct a model of their environment represented by a variable \mathbf{y} , e.g., a vector of landmark positions. Each robot i also aims to estimate its own state $\mathbf{x}_{i,t}$, e.g., pose, at time t . The combined state of robot i is denoted as $\mathbf{s}_{i,t} = [\mathbf{x}_{i,t}^\top \mathbf{y}^\top]^\top$ and evolves according to a known Markov motion model:

$$\mathbf{s}_{i,t+1} \sim f_i(\cdot \mid \mathbf{s}_{i,t}, \mathbf{u}_{i,t}), \quad (1)$$

where $\mathbf{u}_{i,t}$ is a control input and f_i is the probability density function (PDF) of the next state $\mathbf{s}_{i,t+1}$. Each robot receives observations $\mathbf{z}_{i,t}$ according to a known observation model:

$$\mathbf{z}_{i,t} \sim h_i(\cdot \mid \mathbf{s}_{i,t}), \quad (2)$$

where h_i is the observation PDF.

The robots communicate over a network represented as a connected undirected graph $\mathcal{G} = (\mathcal{V}, \mathcal{E})$ with nodes $\mathcal{V} = \{1, \dots, n\}$ corresponding to the robots and edges $\mathcal{E} \subseteq \mathcal{V} \times \mathcal{V}$ specifying robot pairs that can exchange information. For example, $(i, j) \in \mathcal{E}$ indicates that robot i and j can exchange information. Let $A \in \mathbb{R}^{n \times n}$ be a doubly stochastic weighted adjacency matrix of \mathcal{G} such that $A_{ij} > 0$ if $(i, j) \in \mathcal{E}$ and $A_{ij} = 0$ otherwise. Also, let $\mathcal{N}_i := \{j \in \mathcal{V} \mid (j, i) \in \mathcal{E}\} \cup \{i\}$ denote the set of one-hop neighbors of robot i . We consider the following problem.

Problem 1. Given control inputs $\mathbf{u}_i = [\mathbf{u}_{i,0}^\top, \dots, \mathbf{u}_{i,T-1}^\top]^\top$ and observations $\mathbf{z}_i := [\mathbf{z}_{i,0}^\top, \dots, \mathbf{z}_{i,T}^\top]^\top$ at each robot i , estimate the robot states $\mathbf{s}_i := [\mathbf{s}_{i,0}^\top, \dots, \mathbf{s}_{i,T}^\top]^\top$ collaboratively by communicating only with one-hop neighbors according to the structure of the graph \mathcal{G} .

IV. DISTRIBUTED VARIATIONAL INFERENCE

We approach the collaborative estimation problem using variational inference. We develop a distributed mirror descent algorithm to estimate a (variational) density of the states $\mathbf{s}_{i,t}$ with regularization that enforces consensus on the estimates of the common landmarks \mathbf{y} among the robots.

A. Variational inference

As shown in [34], a Kalman filter/smoothen can be derived by minimizing the Kullback-Leibler (KL) divergence between a variational density $q_i(\mathbf{s}_i)$ and the true Bayesian posterior $p_i(\mathbf{s}_i|\mathbf{u}_i, \mathbf{z}_i)$. Adopting a Bayesian perspective, the posterior is proportional to the joint density, which factorizes into products of motion and observation likelihoods due to the Markov assumptions in the models (1), (2):

$$\begin{aligned} p_i(\mathbf{s}_i|\mathbf{u}_i, \mathbf{z}_i) &\propto p_i(\mathbf{s}_i, \mathbf{u}_i, \mathbf{z}_i) \\ &\propto p_i(\mathbf{s}_{i,0}) \prod_{t=0}^{T-1} f_i(\mathbf{s}_{i,t+1}|\mathbf{s}_{i,t}, \mathbf{u}_{i,t}) \prod_{t=0}^T h_i(\mathbf{z}_{i,t}|\mathbf{s}_{i,t}). \end{aligned} \quad (3)$$

The KL divergence between the variational density $q_i(\mathbf{s}_i)$ and the true posterior $p_i(\mathbf{s}_i|\mathbf{u}_i, \mathbf{z}_i)$ can be decomposed as:

$$\begin{aligned} \text{KL}(q_i||p_i) &= \mathbb{E}_{q_i}[-\log p_i(\mathbf{s}_i, \mathbf{u}_i, \mathbf{z}_i)] \\ &\quad - \underbrace{\mathbb{E}_{q_i}[-\log q_i(\mathbf{s}_i)]}_{\text{entropy}} + \underbrace{\log p_i(\mathbf{u}_i, \mathbf{z}_i)}_{\text{constant}}, \end{aligned} \quad (4)$$

where for simplicity of notation q_i without input arguments refers to $q_i(\mathbf{s}_i)$. Dropping the constant term, leads to the following optimization problem at robot i :

$$\min_{q_i \in \mathcal{Q}_i} c_i(q_i) := \mathbb{E}_{q_i}[-\log p_i(\mathbf{s}_i, \mathbf{z}_i, \mathbf{u}_i) + \log q_i(\mathbf{s}_i)], \quad (5)$$

where \mathcal{Q}_i is a family of admissible variational densities.

B. Distributed mirror descent

The variational inference problem in (5) can be solved using the mirror descent algorithm [7]. Mirror descent is a generalization of projected gradient descent that performs projection using a generalized distance (Bregman divergence), instead of the usual Euclidean distance, to respect the geometry of the constraint set \mathcal{Q}_i . Since \mathcal{Q}_i is a space of PDFs, a suitable choice of Bregman divergence is the KL divergence. Starting with a prior PDF $q_i^{(0)}(\mathbf{s}_i)$, the mirror descent algorithm performs the following iterations:

$$q_i^{(k+1)} \in \arg \min_{q_i \in \mathcal{Q}_i} \mathbb{E}_{q_i} \left[\frac{\delta c_i}{\delta q_i}(q_i^{(k)}) \right] + \frac{1}{\alpha_k} \text{KL}(q_i||q_i^{(k)}), \quad (6)$$

where $\delta c_i/\delta q_i(q_i^{(k)})$ is the Fréchet derivative of $c_i(q_i)$ with respect to q_i evaluated at $q_i^{(k)}$ and $\alpha_k > 0$ is a step size.

Note that the optimizations (6) at each robot i are completely decoupled and, hence, each robot would be estimating

its own density over the common landmarks \mathbf{y} . To make the estimation process collaborative, the regularization term $\text{KL}(q_i||q_i^{(k)})$ in (6) should require that the PDF q_i of robot i is also similar to the priors $q_j^{(k)}$ of its neighbors \mathcal{N}_i rather than its own prior $q_i^{(k)}$ alone. This idea was introduced in the distributed mirror descent algorithm in [35], where a weighted sum of KL divergences with respect to each neighbor is used for regularization. In our case, the PDFs $q_j^{(k)}(\mathbf{s}_j) = q_j^{(k)}(\mathbf{x}_j, \mathbf{y})$ are not defined over the same set of variables since each robot j is estimating its own private state \mathbf{x}_j as well. To enforce consensus only on the common state \mathbf{y} , the KL divergence term in (6) can be decomposed as a sum of marginal and conditional terms:

$$\begin{aligned} \text{KL}(q_i(\mathbf{x}_i, \mathbf{y})||q_i^{(k)}(\mathbf{x}_i, \mathbf{y})) &= \text{KL}(q_i(\mathbf{y})||q_i^{(k)}(\mathbf{y})) \\ &\quad + \text{KL}(q_i(\mathbf{x}_i|\mathbf{y})||q_i^{(k)}(\mathbf{x}_i|\mathbf{y})). \end{aligned} \quad (7)$$

Hence, we can regularize only the marginal density $q_i(\mathbf{y})$ of the common environment state \mathbf{y} to remain similar to the marginal densities $q_j^{(k)}(\mathbf{y})$ of the one-hop neighbors by using a weighted sum of KL divergences. This leads to the following optimization problem at robot i :

$$\begin{aligned} q_i^{(k+1)} &\in \arg \min_{q_i \in \mathcal{Q}_i} g_i(q_i) \\ g_i(q_i) &:= \mathbb{E}_{q_i} \left[\frac{\delta c_i}{\delta q_i}(q_i^{(k)}) \right] + \frac{1}{\alpha^{(k)}} \text{KL}(q_i(\mathbf{x}_i|\mathbf{y})||q_i^{(k)}(\mathbf{x}_i|\mathbf{y})) \\ &\quad + \frac{1}{\alpha^{(k)}} \sum_{j \in \mathcal{N}_i} A_{ij} \text{KL}(q_i(\mathbf{y})||q_j^{(k)}(\mathbf{y})), \end{aligned} \quad (8)$$

where $\mathcal{Q}_i = \{q_i \mid \int q_i = 1\}$ is the feasible set and A_{ij} are the elements of the adjacency matrix with $\sum_{j \in \mathcal{N}_i} A_{ij} = 1$. We derive a closed-form expression for the optimizer in the following proposition.

Proposition 1. *The optimizers of (8) satisfy:*

$$\begin{aligned} q_i^{(k+1)}(\mathbf{x}_i, \mathbf{y}) &\propto [p_i(\mathbf{x}_i, \mathbf{y}, \mathbf{z}_i, \mathbf{u}_i)/q_i^{(k)}(\mathbf{x}_i, \mathbf{y})]^{\alpha_k} \\ &\quad q_i^{(k)}(\mathbf{x}_i|\mathbf{y}) \prod_{j \in \mathcal{N}_i} [q_j^{(k)}(\mathbf{y})]^{A_{ij}}. \end{aligned} \quad (9)$$

Proof. See Appendix A. \square

C. Linear Gaussian case

In this section, we consider linear Gaussian models and obtain an explicit form of the distributed variational inference update in (9). Suppose each robot i has the following motion and observation models:

$$\begin{aligned} \mathbf{s}_{i,t+1} &= F_i \mathbf{s}_{i,t} + G_i \mathbf{u}_{i,t} + \mathbf{w}_{i,t}, & \mathbf{w}_{i,t} &\sim \mathcal{N}(\mathbf{0}, W_i), \\ \mathbf{z}_{i,t} &= H_i \mathbf{s}_{i,t} + \mathbf{v}_{i,t}, & \mathbf{v}_{i,t} &\sim \mathcal{N}(\mathbf{0}, V_i). \end{aligned} \quad (10)$$

Let the prior density of $\mathbf{s}_{i,0}$ be $\mathcal{N}(\boldsymbol{\mu}_{i,0}, \Sigma_{i,0})$ and considering all timesteps, we can write the models in lifted form as

$$\begin{aligned} \mathbf{s}_i &= \bar{F}_i(\bar{G}_i \mathbf{u}_i + \bar{\mathbf{w}}_i), & \bar{\mathbf{w}}_i &\sim \mathcal{N}(\mathbf{0}, \bar{W}_i), \\ \mathbf{z}_i &= \bar{H}_i \mathbf{s}_i + \bar{\mathbf{v}}_i, & \bar{\mathbf{v}}_i &\sim \mathcal{N}(\mathbf{0}, \bar{V}_i), \end{aligned} \quad (11)$$

with the lifted terms defined as below

$$\begin{aligned} \mathbf{s}_i &= [\mathbf{s}_{i,0}^\top \cdots \mathbf{s}_{i,T}^\top]^\top, \quad \mathbf{u}_i^\top = [\boldsymbol{\mu}_{i,0}^\top \mathbf{u}_{i,0} \cdots \mathbf{u}_{i,T}^\top]^\top, \\ \mathbf{z}_i &= [\mathbf{z}_{i,0}^\top \cdots \mathbf{z}_{i,T}^\top]^\top, \quad \bar{H}_i = I_{T+1} \otimes H_i, \\ \bar{V}_i &= I_{T+1} \otimes V_i, \quad \bar{W}_i = \begin{bmatrix} \Sigma_{i,0} & 0 \\ 0 & I_T \otimes W_i \end{bmatrix}, \\ \bar{F}_i &= \begin{bmatrix} I & 0 & \cdots & 0 \\ F & I & \cdots & 0 \\ \vdots & \vdots & \ddots & \vdots \\ F^{T-1} & F^{T-2} & \cdots & I \end{bmatrix}, \quad \bar{G}_i = \begin{bmatrix} I & 0 \\ 0 & I_T \otimes G_i \end{bmatrix}, \end{aligned} \quad (12)$$

Denoting the density and distribution at iteration k as $q_i^{(k)}(\mathbf{s}_i)$ and $\mathcal{N}(\boldsymbol{\mu}_{i,(k)}, \Sigma_{i,(k)})$, the distributed variational inference update in (9) is computed in the following propositions.

Proposition 2. Consider a joint Gaussian distribution

$$\begin{bmatrix} \mathbf{x} \\ \mathbf{y} \end{bmatrix} \sim \mathcal{N} \left(\begin{bmatrix} \boldsymbol{\mu}^x \\ \boldsymbol{\mu}^y \end{bmatrix}, \begin{bmatrix} \Sigma^x & \Sigma^{xy} \\ \Sigma^{xy^\top} & \Sigma^y \end{bmatrix} \right). \quad (13)$$

If the marginal distribution over \mathbf{y} changes to $\mathcal{N}(\bar{\boldsymbol{\mu}}^y, \bar{\Sigma}^y)$, the new joint distribution $\mathcal{N}(\bar{\boldsymbol{\mu}}, \bar{\Sigma})$ of (\mathbf{x}, \mathbf{y}) will be

$$\begin{aligned} \bar{\boldsymbol{\mu}} &= \begin{bmatrix} A\bar{\boldsymbol{\mu}}^y + \mathbf{b} \\ \bar{\boldsymbol{\mu}}^y \end{bmatrix}, \quad \bar{\Sigma} = \begin{bmatrix} A\bar{\Sigma}^y A^\top + P & A\bar{\Sigma}^y \\ \bar{\Sigma}^y A^\top & \bar{\Sigma}^y \end{bmatrix}, \\ A &= \Sigma^{xy} \Sigma^{y-1}, \quad \mathbf{b} = \boldsymbol{\mu}^x - \Sigma^{xy} \Sigma^{y-1} \boldsymbol{\mu}^y, \\ P &= \Sigma^x - \Sigma^{xy} \Sigma^{y-1} \Sigma^{xy^\top}. \end{aligned} \quad (14)$$

Proposition 3. In the linear Gaussian case, the distributed variational inference update in (9) can be obtained by first averaging marginal densities of the common state \mathbf{y} across the neighbors \mathcal{N}_i of robot i :

$$\bar{\Sigma}_{i,(k)}^{y-1} = \sum_{j \in \mathcal{N}_i} A_{ij} \Sigma_{j,(k)}^{y-1}, \quad \bar{\Sigma}_{i,(k)}^{y-1} \bar{\boldsymbol{\mu}}_{i,(k)}^y = \sum_{j \in \mathcal{N}_i} A_{ij} \Sigma_{j,(k)}^{y-1} \boldsymbol{\mu}_{j,(k)}^y, \quad (15)$$

then constructing a new joint distribution $\mathcal{N}(\bar{\boldsymbol{\mu}}_{i,(k)}, \bar{\Sigma}_{i,(k)})$ according to Proposition 2, and finally updating the density using the motion and observation models in (11):

$$\begin{aligned} \Sigma_{i,(k+1)}^{-1} &= \bar{\Sigma}_{i,(k)}^{-1} + \alpha_k (\bar{F}_i^{-\top} \bar{W}_i^{-1} \bar{F}_i^{-1} + \bar{H}_i^\top \bar{V}_i^{-1} \bar{H}_i - \Sigma_{i,(k)}^{-1}), \\ \Sigma_{i,(k+1)}^{-1} \boldsymbol{\mu}_{i,(k+1)} &= \bar{\Sigma}_{i,(k)}^{-1} \bar{\boldsymbol{\mu}}_{i,(k)} \\ &+ \alpha_k (\bar{F}_i^{-\top} \bar{W}_i^{-1} \bar{G}_i \mathbf{u}_i + \bar{H}_i^\top \bar{V}_i^{-1} \mathbf{z}_i - \Sigma_{i,(k)}^{-1} \boldsymbol{\mu}_{i,(k)}). \end{aligned} \quad (16)$$

Proof. See Appendix B. \square

In the above proposition, the averaging over the marginal densities in (15) comes from the term $\prod_{j \in \mathcal{N}_i} [q_j^{(k)}(\mathbf{y})]^{A_{ij}}$ in (9), which enforces consensus among the robots over the common variables \mathbf{y} . If the robots are in consensus, i.e., $\boldsymbol{\mu}_{i,(k)}^y = \boldsymbol{\mu}_{j,(k)}^y$, $\Sigma_{i,(k)}^y = \Sigma_{j,(k)}^y$, $\forall j \in \mathcal{N}_i$, (16) with $\alpha_k = 1$ converges in just one step,

$$\begin{aligned} \Sigma_i^{-1} &= \bar{F}_i^{-\top} \bar{W}_i^{-1} \bar{F}_i^{-1} + \bar{H}_i^\top \bar{V}_i^{-1} \bar{H}_i, \\ \Sigma_i^{-1} \boldsymbol{\mu}_i &= \bar{F}_i^{-\top} \bar{W}_i^{-1} \bar{G}_i \mathbf{u}_i + \bar{H}_i^\top \bar{V}_i^{-1} \mathbf{z}_i. \end{aligned} \quad (17)$$

As shown in [36, Chapter 3.3], considering only two consecutive time steps in the lifted form in (11) leads to a Kalman filter. Using the result in Proposition 3, we obtain a distributed Kalman filter that incorporates the consensus averaging step in (15).

V. DISTRIBUTED MSCKF

In this section, we use Proposition 3 to derive a distributed version of the MSCKF algorithm [8], summarized in Algorithm 1. Each step of the algorithms is described in the following subsections.

Algorithm 1 Distributed Multi-State Constraint Kalman Filter

Input: Prior mean and covariance $(\boldsymbol{\mu}_{i,t-1}, \Sigma_{i,t-1})$, control input $\mathbf{u}_{i,t-1}$, and measurements $\mathbf{z}_{i,t}^g, \mathbf{z}_{i,t}^o$.

Output: Posterior mean and covariance $(\boldsymbol{\mu}_{i,t}, \Sigma_{i,t})$

1: **Consensus averaging:** (19), (21) in Sec. V-B

2: **State propagation:** (22), (23) in Sec. V-C

3: **State update:** (25), (26) in Sec. V-D

4: **Feature initialization:** (28) in Sec. V-E

A. State and observation description

The state $\mathbf{s}_{i,t}$ of robot i at time t contains a sequence of c historical camera poses $\mathbf{x}_{i,t}$ and a set of m_t landmarks $\mathbf{y}_{i,t}$:

$$\begin{aligned} \mathbf{s}_{i,t} &= (\mathbf{x}_{i,t}, \mathbf{y}_{i,t}), \\ \mathbf{x}_{i,t} &= (T_{i,t-c+1}, \dots, T_{i,t}), \quad T_{i,k} \in SE(3), \quad \forall k, \\ \mathbf{y}_{i,t} &= [\mathbf{p}_{i,1}^\top \cdots \mathbf{p}_{i,m_t}^\top]^\top, \quad \mathbf{p}_{i,k} \in \mathbb{R}^3, \quad \forall k. \end{aligned} \quad (18)$$

Besides the joint mean of the historical camera poses $\mathbf{x}_{i,t}$ and landmarks $\mathbf{y}_{i,t}$, each robot also keeps track a joint covariance $\Sigma_{i,t} \in \mathbb{R}^{(6c+3m_t) \times (6c+3m_t)}$. Each robot obtains observations $\mathbf{z}_{i,t}^o$ of persistent features, e.g., object detections, and observations $\mathbf{z}_{i,t}^g$ of opportunistic features, e.g., image keypoints or visual features, as illustrated in Fig. 1. We use point observations and the pinhole camera model for both feature types. Only the landmarks associated with persistent features are initialized and stored in the state while the landmarks associated with opportunistic features are used for structureless updates as in the MSCKF algorithm [8].

B. Consensus averaging

Each robot i communicates with its neighbors \mathcal{N}_i to find out common landmarks. Then each robot sends the mean and covariance of the common landmarks $\boldsymbol{\mu}_{i,t-1}^y, \Sigma_{i,t-1}^y$ to its neighbors and receives $\boldsymbol{\mu}_{j,t-1}^y, \Sigma_{j,t-1}^y$, $j \in \mathcal{N}_i \setminus \{i\}$. The consensus averaging step is carried out by averaging the marginal distributions of the common landmarks:

$$\begin{aligned} \bar{\Sigma}_{i,t-1}^{y-1} &= \sum_{j \in \mathcal{N}_i} A_{ij} \Sigma_{j,t-1}^{y-1}, \\ \bar{\Sigma}_{i,t-1}^{y-1} \bar{\boldsymbol{\mu}}_{i,t-1}^y &= \sum_{j \in \mathcal{N}_i} A_{ij} \Sigma_{j,t-1}^{y-1} \boldsymbol{\mu}_{j,t-1}^y, \end{aligned} \quad (19)$$

which is the same as (15) except that we only consider one time step t here. Then, we need to reconstruct the new joint distribution $\mathcal{N}(\bar{\boldsymbol{\mu}}_{i,t-1}, \bar{\Sigma}_{i,t-1})$. Since we store the historical camera poses as $SE(3)$ matrices, Proposition 2 can not be applied directly. Following [36, Chapter 7.3.1], we define a Gaussian distribution over a historical camera pose $T_{i,k}$, $k = t-c, \dots, t-1$ by adding a perturbation $\epsilon_{i,k}$:

$$T_{i,k} = T_{i,k} \exp(\epsilon_{i,k}^\wedge), \quad \epsilon_{i,k} \sim \mathcal{N}(\mathbf{0}_6, \Sigma_{i,t-1}^{x_k}), \quad (20)$$

where $(\cdot)^\wedge$ defined in [36, Chapter 7.1.2] converts from \mathbb{R}^6 to a $\mathbb{R}^{4 \times 4}$ twist matrix. The estimated covariance $\Sigma_{i,t-1}$ already takes account of both the poses and landmarks. For consistency of notation with Proposition 2, we denote the mean of the pose perturbation as $\boldsymbol{\mu}_{i,t-1}^x = \mathbf{0}_{6c}$. After averaging and reconstructing the new joint distribution, $\bar{\boldsymbol{\mu}}_{i,t-1}^x$ may be non-zero, so we need to correct the camera poses as follows:

$$\bar{T}_{i,k} = T_{i,k} \exp(\bar{\boldsymbol{\mu}}_{i,t-1}^x \wedge), \quad \bar{\boldsymbol{\mu}}_{i,t-1}^x \in \mathbb{R}^6, \quad k = t-c, \dots, t-1. \quad (21)$$

C. State propagation

We derive a general odometry propagation step for the MSCKF algorithm, thus not necessarily requiring IMU measurements and enabling vision-only propagation. We assume an odometry algorithm (e.g., libviso2 [37]) provides a relative pose measurement $\delta T_{i,t-1}$ between the previous frame at time $t-1$ and the current frame at time t . The state at each robot i is propagated as:

$$\begin{aligned} \mathbf{x}_{i,t}^+ &= (\bar{T}_{i,t-c+1}, \dots, \bar{T}_{i,t-1}, \bar{T}_{i,t-1} \delta T_{i,t-1}), \\ \mathbf{s}_{i,t}^+ &= (\mathbf{x}_{i,t}^+, \bar{\boldsymbol{\mu}}_{i,t-1}^y), \end{aligned} \quad (22)$$

where the terms $(\bar{\cdot})$ are obtained from the consensus averaging step. The state covariance is propagated as follows:

$$\begin{aligned} \Sigma_{i,t}^+ &= \begin{bmatrix} A & 0 \\ J_t & 0 \\ 0 & I_{3m_{t-1}} \end{bmatrix} \bar{\Sigma}_{i,t-1} \begin{bmatrix} A & 0 \\ J_t & 0 \\ 0 & I_{3m_{t-1}} \end{bmatrix}^\top + \text{diag}(\mathbf{e}_{6n}) \otimes W_i, \\ A &= [0_{6(c-1) \times 6} | I_{6(c-1)}], \quad J_t = [0_{6 \times 6(c-1)} \text{Ad}(\delta T_{i,t-1}^{-1})], \end{aligned} \quad (23)$$

where $\text{Ad}(\cdot)$ is the adjoint of an $SE(3)$ matrix [36, Chapter 7.1.4], $\mathbf{e}_{6n} \in \mathbb{R}^{6n+3m_t}$ is a vector with the $6n$ -th element as 1 and the rest as 0, and $W_i \in \mathbb{R}^{6 \times 6}$ is the odometry measurement covariance.

D. State update

The MSCKF update step follows the previous work [38]. We first define several residuals. The camera pose residual is a perturbation $\underline{\epsilon}_{i,k}$ that transforms the estimated pose $T_{i,k}$ to the true pose $\underline{T}_{i,k}$, i.e. $\underline{T}_{i,k} = T_{i,k} \exp(\underline{\epsilon}_{i,k} \wedge)$. The landmark residual is the difference between true position $\underline{\mathbf{p}}$ and the estimated position $\hat{\mathbf{p}}$, i.e., $\tilde{\mathbf{p}} = \underline{\mathbf{p}} - \hat{\mathbf{p}}$, where $\hat{\mathbf{p}}$ is the position mean if the landmark is in the state or the result triangulation if it is not. When robot i receives the k -th geometric feature observation at time t , denoted as $\mathbf{z}_{i,t,k}^g$, we linearize the observation model around the current error state $\tilde{\mathbf{s}}_{i,t,k}$ (composed of both pose and landmark residuals) and the feature position residual $\tilde{\mathbf{p}}_{i,k}^g$:

$$\mathbf{r}_{i,t,k}^g = \mathbf{z}_{i,t,k}^g - \hat{\mathbf{z}}_{i,t,k}^g = H_{i,t,k}^{\mathbf{s},g} \tilde{\mathbf{s}}_{i,t,k} + H_{i,t,k}^{\mathbf{p},g} \tilde{\mathbf{p}}_{i,k}^g + \mathbf{v}_{i,t,k}^g,$$

where $\hat{\mathbf{z}}_{i,t,k}^g$ is the predicted observation based on the observation model and $H_{i,t,k}^{\mathbf{s},g}$ and $H_{i,t,k}^{\mathbf{p},g}$ are Jacobians. Then, we left-multiply by the nullspace $N_{i,t,k}$ of $H_{i,t,k}^{\mathbf{p},g}$ to remove the effect of $\tilde{\mathbf{p}}_{i,k}^g$:

$$\mathbf{r}_{i,t,k}^{g,0} = N_{i,t,k}^\top \mathbf{r}_{i,t,k}^g = N_{i,t,k}^\top H_{i,t,k}^{\mathbf{s},g} \tilde{\mathbf{s}}_{i,t,k} + N_{i,t,k}^\top \mathbf{v}_{i,t,k}^g. \quad (24)$$

Concatenating $\mathbf{r}_{i,t,k}^{g,0}$, $N_{i,t,k}^\top H_{i,t,k}^{\mathbf{s},g}$ for all k , we get an overall geometric feature residual $\mathbf{r}_{i,t}^g$ and Jacobian $H_{i,t}^g$.

Similarly, we linearize the observation model for the object features $\mathbf{z}_{i,t,k}^o$:

$$\mathbf{r}_{i,t,k}^o = \mathbf{z}_{i,t,k}^o - \hat{\mathbf{z}}_{i,t,k}^o = H_{i,t,k}^{\mathbf{s},o} \tilde{\mathbf{s}}_{i,t} + \mathbf{v}_{i,t,k}^o, \quad \mathbf{v}_{i,t,k}^o \sim \mathcal{N}(\mathbf{0}, V_i^o),$$

and concatenate $\mathbf{r}_{i,t,k}^o$ and $H_{i,t,k}^{\mathbf{s},o}$ for all k to get an overall object observation residual $\mathbf{r}_{i,t}^o$ and Jacobian $H_{i,t}^o$.

Finally, by concatenating the residuals and Jacobians of both geometric and object features, we get the overall residual $\mathbf{r}_{i,t} = [\mathbf{r}_{i,t}^g \mathbf{r}_{i,t}^o]^\top$ and Jacobian $H_{i,t} = [H_{i,t}^g \ H_{i,t}^o]^\top$ and compute the Kalman gain:

$$K_{i,t} = \Sigma_{i,t}^+ H_{i,t}^\top (H_{i,t} \Sigma_{i,t}^+ H_{i,t}^\top + I \otimes V_i)^{-1}, \quad (25)$$

where $\Sigma_{i,t}^+$ comes from the propagation step and $K_{i,t}$ can be split to $K_{i,t}^x$ and $K_{i,t}^y$ related to $\mathbf{x}_{i,t}$ and $\mathbf{y}_{i,t}$ respectively. The landmark mean, camera poses, and the entire covariance are updated as:

$$\begin{aligned} \boldsymbol{\mu}_{i,t}^y &= \boldsymbol{\mu}_{i,t}^{y+} + K_{i,t}^y \mathbf{r}_{i,t}, \\ T_{i,k} &= T_{i,k}^+ \exp(K_{i,t}^x \mathbf{r}_{i,t}), \quad K_{i,t}^x \mathbf{r}_{i,t} \in \mathbb{R}^6, \quad k = t-c+1, \dots, t, \\ \Sigma_{i,t} &= (I - K_{i,t} H_{i,t}) \Sigma_{i,t}^+ \end{aligned} \quad (26)$$

where the terms $(\cdot)^+$ are from the propagation step.

E. Feature initialization

The feature initialization is the same as [39]. To initialize an object landmark, we first linearize the observation model

$$\tilde{\mathbf{z}}_{i,t,k}^o = H_{i,t,k}^{\mathbf{s}} \tilde{\mathbf{s}}_{i,t} + H_{i,t,k}^{\mathbf{p}} \tilde{\mathbf{p}}_{i,k}^o + \mathbf{v}_{i,t,k}^o, \quad \mathbf{v}_{i,t,k}^o \sim \mathcal{N}(\mathbf{0}, V_i^o),$$

where $\tilde{\mathbf{z}}_{i,t,k}^o$, $\tilde{\mathbf{s}}_{i,t}$ and $\tilde{\mathbf{p}}_{i,k}^o$ are the residuals of the observation, current state, and new landmark respectively. Then, QR decomposition is performed to separate the linearized observation model into two parts: one that depends on the new landmark and another that does not:

$$\begin{bmatrix} \tilde{\mathbf{z}}_{i,t,k}^{o,1} \\ \tilde{\mathbf{z}}_{i,t,k}^{o,2} \end{bmatrix} = \begin{bmatrix} H_{i,t,k}^{\mathbf{s},1} & H_{i,t,k}^{\mathbf{p},1} \\ H_{i,t,k}^{\mathbf{s},2} & 0 \end{bmatrix} \begin{bmatrix} \tilde{\mathbf{s}}_{i,t} \\ \tilde{\mathbf{p}}_{i,k}^o \end{bmatrix} + \begin{bmatrix} \mathbf{v}_{i,t,k}^{o,1} \\ \mathbf{v}_{i,t,k}^{o,2} \end{bmatrix}. \quad (27)$$

In this way, we can augment the current state and covariance matrix as follows:

$$\begin{aligned} \mathbf{p}_{i,k}^o &= \hat{\mathbf{p}}_{i,k}^o + H_{i,t,k}^{\mathbf{s},1-1} \tilde{\mathbf{z}}_{i,t,k}^{o,1}, \\ \Sigma_{i,t,k}^{\mathbf{sp}} &= -\Sigma_{i,t} H_{i,t,k}^{\mathbf{s},1\top} H_{i,t,k}^{\mathbf{p},1-1\top}, \\ \Sigma_{i,t,k}^{\mathbf{p}} &= H_{i,t,k}^{\mathbf{p},1-1} (H_{i,t,k}^{\mathbf{s},1} \Sigma_{i,t} H_{i,t,k}^{\mathbf{s},1\top} + V_i^{o,1}) H_{i,t,k}^{\mathbf{p},1-1\top}, \end{aligned} \quad (28)$$

where $V_i^{o,1}$ is the covariance of noise $\mathbf{v}_{i,t,k}^{o,1}$, $\Sigma_{i,t,k}^{\mathbf{sp}}$ is the cross-correlation term between the current state and new landmark, and $\Sigma_{i,t,k}^{\mathbf{p}}$ is the covariance of the new landmark.

VI. EVALUATION

We implement our distributed MSCKF algorithm with only stereo visual inputs and evaluate it by conducting experiments using the real-world KITTI dataset [40] and simulated data involving a larger number of robots.

A. KITTI dataset

The KITTI dataset [40] is an autonomous driving dataset that provides stereo images, LiDAR point clouds, and annotated ground-truth robot trajectories. We provide details about the data processing and evaluation results below.

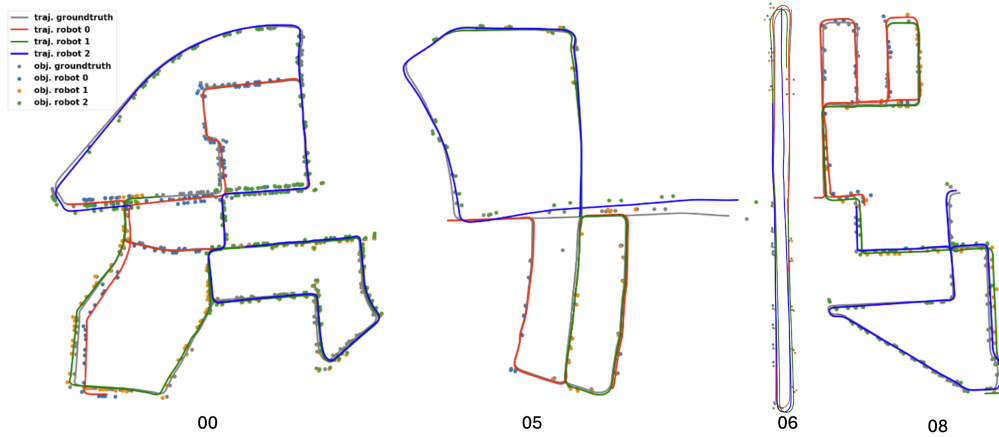


Fig. 2: Visualization of the trajectory and object estimates obtained by 3 robots on KITTI sequences 00, 05, 06 and 08.

1) *Sequences and splits*: We chose long sequences in the KITTI odometry dataset with loop closures and a sufficient number of cars, used as object landmarks, namely, sequences 00, 05, 06, and 08. Each sequence is split into 3 sub-sequences representing 3 different robots. The sequence splits are as follows: sequence 00: [0, 2000], [1500, 3500], [2500, 4540]; sequence 05: [0, 1200], [800, 2000], [1560, 2760]; sequence 06: [0, 700], [200, 900], [400, 1100]; sequence 08: [0, 2000], [1000, 3000], [2000, 4070]. We used a fully connected graph and the adjacency matrix $A \in \mathbb{R}^{3 \times 3}$ has all elements as $\frac{1}{3}$.

2) *Geometric features*: Same as [38], we extract geometric features using the FAST corner detector [5]. The KLT optical flow algorithm [41] is applied to track the features temporally and match them across stereo images. Outlier rejection is performed using 2-point RANSAC for temporal tracking and the known essential matrix for stereo matching. Finally, circular matching similar to [42] is performed to further remove outliers.

3) *Object features*: We utilize YOLOv6 [6] to detect object bounding boxes and compute the centers as our object observations. Since our work does not focus on object tracking, we directly use the instance ID annotations in SemanticKITTI [43] for data association. The instance annotations are provided for LiDAR point clouds and we associate them with the bounding boxes by projecting the LiDAR point clouds onto the image plane and checking the dominant instance points inside each bounding box.

4) *Odometry*: The relative pose $\delta T_{i,t}$ between consecutive camera frames is obtained by LIBVISO2 [37].

5) *Results and analysis*: Qualitative results from three-robot collaborative object SLAM on the KITTI dataset are shown in Fig. 2. We show the root mean square error (RMSE) of the robot trajectory estimates in Table I and the mean distances between estimated object positions and the ground truth in Table II. We do use alignment for the trajectory RMSE [44] because trajectory transformations affect the object mapping errors. We can see that, although consensus averaging can harm the estimation accuracy for some robots compared to running individual MSCKF algorithms at each

TABLE I: Trajectory RMSE in meters on KITTI sequences. Separate and consensus correspond to without/with the consensus averaging step in Sec. V-B.

| | Robot 1 | Robot 2 | Robot 3 | Avg | Max |
|--------------|--------------|--------------|-------------|--------------|--------------|
| 00 Separate | 12.47 | 7.55 | 12.42 | 10.81 | 12.47 |
| 00 Consensus | 12.51 | 7.13 | 8.73 | 9.45 | 12.51 |
| 05 Separate | 7.17 | 10.53 | 10.06 | 9.26 | 10.53 |
| 05 Consensus | 4.69 | 7.75 | 9.56 | 7.33 | 9.56 |
| 06 Separate | 4.23 | 5.60 | 4.86 | 4.90 | 5.60 |
| 06 Consensus | 4.23 | 5.61 | 4.76 | 4.87 | 5.61 |
| 08 Separate | 15.08 | 24.28 | 9.18 | 16.18 | 24.28 |
| 08 Consensus | 13.89 | 12.71 | 9.18 | 11.93 | 13.89 |

TABLE II: Object estimation errors in meters on KITTI sequences. Separate and consensus correspond to without/with the consensus averaging step in Sec. V-B.

| | Robot 1 | Robot 2 | Robot 3 | Avg | Max |
|--------------|--------------|--------------|-------------|--------------|--------------|
| 00 Separate | 8.76 | 7.61 | 8.70 | 8.36 | 8.76 |
| 00 Consensus | 9.30 | 6.74 | 7.16 | 7.73 | 9.30 |
| 05 Separate | 6.08 | 8.54 | 8.82 | 7.82 | 8.82 |
| 05 Consensus | 4.56 | 7.51 | 8.54 | 6.87 | 8.54 |
| 06 Separate | 3.43 | 5.92 | 4.64 | 4.66 | 5.92 |
| 06 Consensus | 3.78 | 5.63 | 4.37 | 4.59 | 5.63 |
| 08 Separate | 12.14 | 21.91 | 8.19 | 14.08 | 21.91 |
| 08 Consensus | 12.11 | 13.71 | 9.21 | 11.68 | 13.71 |

robot, it helps improve the overall team performance in terms of both localization and object mapping. Intuitively, the performance of the best robot in the team is sacrificed to improve the overall team performance in localization and mapping. The distributed MSCKF achieves better agreement in the map estimates among the different robots. Although it might be obvious that the map differences reduce with consensus averaging, we still compare the average object position differences with and without averaging in Table III to quantify the reduction in disagreement. We also claim that the consensus averaging step does not add much time overhead because the robots communicate only common landmarks, meaning that the corresponding covariance $\Sigma_{i,t}^y$ in (19) is small, and only perform the averaging with the one-hop communication neighbors. The computation time used by different components in the algorithm is shown in Fig. 3. We can see that consensus averaging takes a small portion

TABLE III: Object position differences in meters across different robots on KITTI sequences. Separate and consensus correspond to without/with the consensus averaging step in Sec. V-B.

| | Robot 1 | Robot 2 | Robot 3 | Avg | Max |
|--------------|-------------|-------------|--------------|-------------|--------------|
| 00 Separate | 9.69 | 10.35 | 8.35 | 9.46 | 10.35 |
| 00 Consensus | 5.95 | 8.62 | 5.11 | 6.56 | 8.62 |
| 05 Separate | 7.25 | 10.20 | 15.74 | 11.06 | 15.74 |
| 05 Consensus | 1.50 | 5.15 | 10.17 | 5.61 | 10.17 |
| 06 Separate | 5.56 | 4.97 | 4.79 | 5.12 | 5.56 |
| 06 Consensus | 5.01 | 4.68 | 4.43 | 4.71 | 5.01 |
| 08 Separate | 14.61 | 20.24 | 23.81 | 19.55 | 23.81 |
| 08 Consensus | 6.50 | 9.48 | 11.36 | 9.12 | 11.36 |

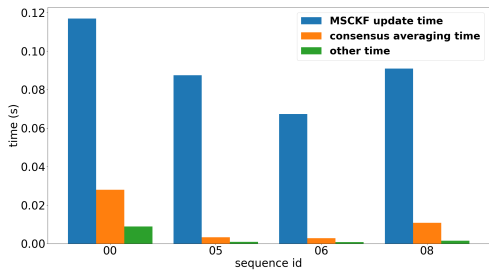


Fig. 3: Time consumed by different components per robot per frame, including MSCKF update, consensus averaging, and other (prediction and landmark initialization).

of time compared with the MSCKF update.

B. Simulated data

To test the performance of our algorithm with increasing numbers of robots, we generated simulated data for 3-15 robots.

1) *Data generation*: Each robot moves along a Lissajous curve and odometry measurements are generated by adding perturbations to the relative transformation between consecutive poses. The landmarks, both geometric and objects, are generated by randomly sampling from Gaussian distributions centered at each trajectory point. There are 210 objects in the scene with different numbers of robots. The observations are then generated by projecting the corresponding landmarks onto the image plane and adding noise.

2) *Results*: A visualization of the simulation result is provided in Fig. 4. The quantitative results from the simulations with fully connected graph are shown in Table IV. We can see that our algorithm scales efficiently with an increasing number of robots in the team while continuing to outperform decoupled MSCKF algorithms run at each robot individually. We also analyze the effect of connectivity in Fig. 5. In the experiment, each robot loses communication with each neighbor according to a certain rate. We can see that our algorithm is robust to communication lost rate up to 0.9. We see that with small numbers of robots (3 and 5), the errors oscillate as the lost rate increases but with relatively large numbers of robots (10 and 15), the errors seem to decrease as the lost rate increases. Analyzing the effect of randomly connected graphs e.g. broad gossip [45] can be future work.

VII. CONCLUSION

We developed a distributed vision-only filtering approach for multi-robot object SLAM. Our experiments demonstrate



Fig. 4: Visualization of the trajectory and object estimates obtained by 15 robots in simulation.

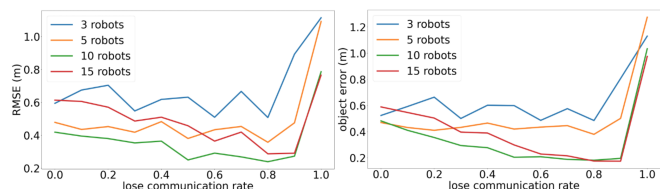


Fig. 5: Analysis of the effect of the robot network connectivity.

TABLE IV: Trajectory, object errors in meters and consensus averaging time per robot per timestep in seconds in simulation with different numbers of robots. Separate and consensus correspond to without/with the consensus averaging step in Sec. V-B.

| Number of robots | 3 | 5 | 10 | 15 |
|-------------------------------|--------------|--------------|--------------|--------------|
| Separate trajectory RMSE (m) | 1.114 | 1.091 | 0.786 | 0.766 |
| Consensus trajectory RMSE (m) | 0.594 | 0.479 | 0.419 | 0.614 |
| Separate object error (m) | 1.131 | 1.275 | 1.034 | 0.975 |
| Consensus object error (m) | 0.524 | 0.470 | 0.482 | 0.589 |
| Consensus averaging time (s) | 0.021 | 0.022 | 0.026 | 0.028 |

that the method improves both localization and mapping accuracy while achieving agreement among the robots on a common object map. Since the algorithm is fully distributed, it allows efficient scaling of the number of robots in the team. Having a common object map is useful for collaborative task planning, which we plan to explore in future work.

ACKNOWLEDGMENTS

The authors are grateful to Shubham Kumar, Shrey Kansal, and Kishore Nukala from the University of California San Diego for technical discussions and help with preparing the datasets for the evaluation.

REFERENCES

- [1] C. Cadena, L. Carlone, H. Carrillo, Y. Latif, D. Scaramuzza, J. Neira, I. Reid, and J. J. Leonard, “Past, present, and future of simultaneous localization and mapping: Toward the robust-perception age,” *IEEE Transactions on Robotics*, vol. 32, no. 6, pp. 1309–1332, 2016.
- [2] J. Kinnari, A. Thomas, P. Lusk, K. Kondo, and J. P. How, “SOS-SLAM: Segmentation for Open-Set SLAM in Unstructured Environments,” *arXiv preprint arXiv:2401.04791*, 2024.
- [3] L. A. A. Andersson and J. Nygard, “C-sam: Multi-robot slam using square root information smoothing,” in *IEEE International Conference on Robotics and Automation (ICRA)*, pp. 2798–2805, 2008.
- [4] I. Deutsch, M. Liu, and R. Siegwart, “A framework for multi-robot pose graph SLAM,” in *IEEE International Conference on Real-time Computing and Robotics*, pp. 567–572, 2016.

- [5] M. Trajković and M. Hedley, "Fast corner detection," *Image and vision computing*, vol. 16, no. 2, pp. 75–87, 1998.
- [6] C. Li, L. Li, H. Jiang, K. Weng, Y. Geng, L. Li, Z. Ke, Q. Li, M. Cheng, W. Nie, et al., "Yolov6: A single-stage object detection framework for industrial applications," *arXiv preprint arXiv:2209.02976*, 2022.
- [7] A. Beck and M. Teboulle, "Mirror descent and nonlinear projected subgradient methods for convex optimization," *Operations Research Letters*, vol. 31, no. 3, pp. 167–175, 2003.
- [8] A. I. Mourikis and S. I. Roumeliotis, "A multi-state constraint kalman filter for vision-aided inertial navigation," in *IEEE International Conference on Robotics and Automation*, pp. 3565–3572, 2007.
- [9] M. Kaess, A. Ranganathan, and F. Dellaert, "iSAM: Incremental Smoothing and Mapping," *IEEE Transactions on Robotics (T-RO)*, vol. 24, no. 6, pp. 1365–1378, 2008.
- [10] M. Kaess, H. Johannsson, R. Roberts, V. Ila, J. Leonard, and F. Dellaert, "iSAM2: Incremental Smoothing and Mapping Using the Bayes Tree," *International Journal of Robotics Research (IJRR)*, vol. 31, no. 2, pp. 216–235, 2012.
- [11] G. Huang, "Visual-inertial navigation: A concise review," in *International Conference on Robotics and Automation (ICRA)*, pp. 9572–9582, 2019.
- [12] J. Delmerico and D. Scaramuzza, "A benchmark comparison of monocular visual-inertial odometry algorithms for flying robots," in *IEEE International Conference on Robotics and Automation (ICRA)*, pp. 2502–2509, 2018.
- [13] S. Mokssit, D. B. Licea, B. Guermah, and M. Ghogho, "Deep Learning Techniques for Visual SLAM: A Survey," *IEEE Access*, vol. 11, pp. 20026–20050, 2023.
- [14] I. Abaspor Kazerouni, L. Fitzgerald, G. Dooly, and D. Toal, "A survey of state-of-the-art on visual SLAM," *Expert Systems with Applications*, vol. 205, p. 117734, 2022.
- [15] Y. Tian, K. Khosoussi, D. M. Rosen, and J. P. How, "Distributed certifiably correct pose-graph optimization," *IEEE Transactions on Robotics*, vol. 37, no. 6, pp. 2137–2156, 2021.
- [16] A. Cunningham, M. Paluri, and F. Dellaert, "DDF-SAM: Fully distributed slam using constrained factor graphs," in *IEEE/RSJ International Conference on Intelligent Robots and Systems (IROS)*, pp. 3025–3030, 2010.
- [17] A. Cunningham, V. Indelman, and F. Dellaert, "DDF-SAM 2.0: Consistent distributed smoothing and mapping," in *IEEE International Conference on Robotics and Automation (ICRA)*, pp. 5220–5227, 2013.
- [18] F. Dellaert and M. Kaess, "Square root SAM: Simultaneous localization and mapping via square root information smoothing," *The International Journal of Robotics Research*, vol. 25, no. 12, pp. 1181–1203, 2006.
- [19] S. Choudhary, L. Carlone, C. Nieto, J. Rogers, H. I. Christensen, and F. Dellaert, "Distributed mapping with privacy and communication constraints: Lightweight algorithms and object-based models," *The International Journal of Robotics Research (IJRR)*, vol. 36, no. 12, pp. 1286–1311, 2017.
- [20] Y. Zhang, M. Hsiao, J. Dong, J. Engel, and F. Dellaert, "Mr-isam2: Incremental smoothing and mapping with multi-root bayes tree for multi-robot slam," in *IEEE/RSJ International Conference on Intelligent Robots and Systems (IROS)*, pp. 8671–8678, 2021.
- [21] Y. Tian and J. P. How, "Spectral sparsification for communication-efficient collaborative rotation and translation estimation," *IEEE Transactions on Robotics*, vol. 40, pp. 257–276, 2024.
- [22] Y. Tian, Y. Chang, F. H. Arias, C. Nieto-Granda, J. P. How, and L. Carlone, "Kimera-multi: Robust, distributed, dense metric-semantic slam for multi-robot systems," *IEEE Transactions on Robotics (TRO)*, vol. 38, no. 4, 2022.
- [23] H. Yang, P. Antonante, V. Tzoumas, and L. Carlone, "Graduated non-convexity for robust spatial perception: From non-minimal solvers to global outlier rejection," *IEEE Robotics and Automation Letters*, vol. 5, no. 2, pp. 1127–1134, 2020.
- [24] P.-Y. Lajoie, B. Ramtoula, Y. Chang, L. Carlone, and G. Beltrame, "Door-SLAM: Distributed, online, and outlier resilient slam for robotic teams," *IEEE Robotics and Automation Letters*, vol. 5, no. 2, pp. 1656–1663, 2020.
- [25] J. G. Mangelson, D. Dominic, R. M. Eustice, and R. Vasudevan, "Pairwise consistent measurement set maximization for robust multi-robot map merging," in *IEEE International Conference on Robotics and Automation (ICRA)*, pp. 2916–2923, 2018.
- [26] H. Xu, P. Liu, X. Chen, and S. Shen, "D²SLAM: Decentralized and Distributed Collaborative Visual-inertial SLAM System for Aerial Swarm," *arXiv preprint:2211.01538*, 2022.
- [27] Z. Peng, Y. Xu, M. Yan, and W. Yin, "ARock: An Algorithmic Framework for Asynchronous Parallel Coordinate Updates," *SIAM Journal on Scientific Computing*, vol. 38, no. 5, pp. A2851–A2879, 2016.
- [28] S. Roumeliotis and G. Bekey, "Distributed multirobot localization," *IEEE Transactions on Robotics and Automation*, vol. 18, no. 5, pp. 781–795, 2002.
- [29] S. Thrun, Y. Liu, D. Koller, A. Y. Ng, Z. Ghahramani, and H. Durrant-Whyte, "Simultaneous Localization and Mapping with Sparse Extended Information Filters," *The International Journal of Robotics Research (IJRR)*, vol. 23, no. 7-8, pp. 693–716, 2004.
- [30] G. P. Huang, N. Trawny, A. I. Mourikis, and S. I. Roumeliotis, "On the consistency of multi-robot cooperative localization," in *Robotics: Science and Systems (RSS)*, 2009.
- [31] G. Huang, M. Kaess, and J. J. Leonard, "Consistent unscented incremental smoothing for multi-robot cooperative target tracking," *Robotics and Autonomous Systems*, vol. 69, pp. 52–67, 2015.
- [32] L. Gao, G. Battistelli, and L. Chisci, "Random-Finite-Set-Based Distributed Multirobot SLAM," *IEEE Transactions on Robotics*, vol. 36, no. 6, pp. 1758–1777, 2020.
- [33] P. Zhu, P. Geneva, W. Ren, and G. Huang, "Distributed visual-inertial cooperative localization," in *IEEE/RSJ International Conference on Intelligent Robots and Systems (IROS)*, pp. 8714–8721, 2021.
- [34] T. D. Barfoot, J. R. Forbes, and D. J. Yoon, "Exactly sparse gaussian variational inference with application to derivative-free batch nonlinear state estimation," *The International Journal of Robotics Research*, vol. 39, no. 13, pp. 1473–1502, 2020.
- [35] P. Paritosh, N. Atanasov, and S. Martinez, "Distributed Bayesian estimation of continuous variables over time-varying directed networks," *IEEE Control Systems Letters*, vol. 6, pp. 2545–2550, 2022.
- [36] T. D. Barfoot, *State estimation for robotics*. Cambridge University Press, 2017.
- [37] A. Geiger, J. Ziegler, and C. Stiller, "Stereoscan: Dense 3d reconstruction in real-time," in *Intelligent Vehicles Symposium (IV)*, 2011.
- [38] K. Sun, K. Mohta, B. Pfrommer, M. Watterson, S. Liu, Y. Mulgaonkar, C. J. Taylor, and V. Kumar, "Robust stereo visual inertial odometry for fast autonomous flight," *IEEE Robotics and Automation Letters*, vol. 3, no. 2, pp. 965–972, 2018.
- [39] P. Geneva, K. Eickenhoff, W. Lee, Y. Yang, and G. Huang, "Openvins: A research platform for visual-inertial estimation," in *IEEE International Conference on Robotics and Automation (ICRA)*, pp. 4666–4672, 2020.
- [40] A. Geiger, P. Lenz, and R. Urtasun, "Are we ready for autonomous driving? The KITTI vision benchmark suite," in *IEEE Conference on Computer Vision and Pattern Recognition (CVPR)*, pp. 3354–3361, 2012.
- [41] B. D. Lucas and T. Kanade, "An iterative image registration technique with an application to stereo vision," in *International Joint Conference on Artificial Intelligence (IJCAI)*, vol. 2, pp. 674–679, 1981.
- [42] B. Kitt, A. Geiger, and H. Lategahn, "Visual odometry based on stereo image sequences with ransac-based outlier rejection scheme," in *IEEE Intelligent Vehicles Symposium*, pp. 486–492, 2010.
- [43] J. Behley, M. Garbade, A. Milioto, J. Quenzel, S. Behnke, C. Stachniss, and J. Gall, "SemanticKITTI: A dataset for semantic scene understanding of lidar sequences," in *IEEE/CVF International Conference on Computer Vision (ICCV)*, pp. 9297–9307, 2019.
- [44] Z. Zhang and D. Scaramuzza, "A tutorial on quantitative trajectory evaluation for visual(-inertial) odometry," in *IEEE/RSJ Int. Conf. Intell. Robot. Syst. (IROS)*, 2018.
- [45] T. C. Aysal, M. E. Yildiz, A. D. Sarwate, and A. Scaglione, "Broadcast gossip algorithms for consensus," *IEEE Transactions on Signal Processing*, vol. 57, no. 7, pp. 2748–2761, 2009.
- [46] C. M. Stein, "Estimation of the mean of a multivariate normal distribution," *The Annals of Statistics*, pp. 1135–1151, 1981.
- [47] P. Paritosh, N. Atanasov, and S. Martinez, "Marginal density averaging for distributed node localization from local edge measurements," in *IEEE Conference on Decision and Control (CDC)*, pp. 2404–2410, 2020.
- [48] N. Atanasov, R. Tron, V. M. Preciado, and G. J. Pappas, "Joint estimation and localization in sensor networks," in *IEEE Conference on Decision and Control*, pp. 6875–6882, 2014.

A. Proof of Proposition 1

Taking the constraint $\int q_i = 1$ into account, we consider the Lagrangian:

$$\begin{aligned} \mathcal{L}(q_i, \lambda) = & \mathbb{E}_{q_i} \left[\frac{\delta c_i}{\delta q_i}(q_i^{(k)}) \right] + \frac{1}{\alpha^{(k)}} \text{KL}(q_i(\mathbf{x}_i|\mathbf{y})||q_i^{(k)}(\mathbf{x}_i|\mathbf{y})) \\ & + \sum_{j \in \mathcal{N}_i} \frac{A_{ij}}{\alpha_k} \text{KL}(q_i(\mathbf{y})||q_j^{(k)}(\mathbf{y})) + \lambda \left(\int q_i - 1 \right), \end{aligned}$$

where λ is a multiplier. The variation of \mathcal{L} w.r.t. q_i is:

$$\begin{aligned} \frac{\delta \mathcal{L}}{\delta q_i} = & \frac{\delta c_i}{\delta q_i}(q_i^{(k)}) + \frac{1}{\alpha_k} (1 + \log q_i) - \frac{1}{\alpha_k} \log q_i^{(k)}(\mathbf{x}_i|\mathbf{y}) \\ & - \frac{1}{\alpha_k} \sum_{j \in \mathcal{N}_i} A_{ij} \log q_j^{(k)}(\mathbf{y}) + \lambda \\ = & -\log p_i(\mathbf{x}_i, \mathbf{y}, \mathbf{z}_i, \mathbf{u}_i) + 1 + \log q_i^{(k)} + \frac{1}{\alpha_k} (1 + \log q_i) \\ & - \frac{1}{\alpha_k} \log q_i^{(k)}(\mathbf{x}_i|\mathbf{y}) - \frac{1}{\alpha_k} \sum_{j \in \mathcal{N}_i} A_{ij} \log q_j^{(k)}(\mathbf{y}) + \lambda. \end{aligned}$$

Setting the variation to zero and solving for q_i , leads to:

$$\begin{aligned} q_i = & e^{-1 - \alpha_k - \alpha_k \lambda} [p_i(\mathbf{x}_i, \mathbf{y}, \mathbf{z}_i, \mathbf{u}_i)/q_i^{(k)}(\mathbf{x}_i, \mathbf{y})]^{\alpha_k} \\ & q_i^{(k)}(\mathbf{x}_i|\mathbf{y}) \prod_{j \in \mathcal{N}_i} [q_j^{(k)}(\mathbf{y})]^{A_{ij}} \\ \propto & [p_i(\mathbf{x}_i, \mathbf{y}, \mathbf{z}_i, \mathbf{u}_i)/q_i^{(k)}(\mathbf{x}_i, \mathbf{y})]^{\alpha_k} q_i^{(k)}(\mathbf{x}_i|\mathbf{y}) \prod_{j \in \mathcal{N}_i} [q_j^{(k)}(\mathbf{y})]^{A_{ij}}. \end{aligned}$$

thus completing the proof.

B. Proof of Proposition 3

Suppose that the density $q_i^{(k)}(\mathbf{x}_i, \mathbf{y})$ of $\mathcal{N}(\boldsymbol{\mu}_{i,(k)}, \Sigma_{i,(k)})$ is the joint density at iteration k and the density $q_j^{(k)}(\mathbf{y})$ of $\mathcal{N}(\boldsymbol{\mu}_{j,(k)}, \Sigma_{j,(k)})$ is the marginal density over \mathbf{y} . To save space, we simplify the notation $q_i^{(k)}(\mathbf{x}_i, \mathbf{y})$ as $q_i^{(k)}$. The objective function (8) can be rewritten as

$$\begin{aligned} g_i^{(k)} = & \mathbb{E}_{q_i} \left[\frac{\delta c_i}{\delta q_i}(q_i^{(k)}) \right] + \frac{1}{\alpha_k} \mathbb{E}_{q_i} [\log q_i] - \frac{1}{\alpha_k} \mathbb{E}_{q_i} [\log q_i^{(k)}] \\ & - \frac{1}{\alpha_k} \mathbb{E}_{q_i} [\log q_i(\mathbf{y})] + \frac{1}{\alpha_k} \mathbb{E}_{q_i} [\log q_i^{(k)}(\mathbf{y})] \\ & + \sum_{j \in \mathcal{N}_i} \frac{A_{ij}}{\alpha_k} \mathbb{E}_{q_i} [\log q_i(\mathbf{y})] - \sum_{j \in \mathcal{N}_i} \frac{A_{ij}}{\alpha_k} \mathbb{E}_{q_i} [\log q_j^{(k)}(\mathbf{y})] \\ = & \mathbb{E}_{q_i} \left[\frac{\delta c_i}{\delta q_i}(q_i^{(k)}) \right] - \frac{1}{2\alpha_k} \log |\Sigma_i| - \frac{1}{\alpha_k} \mathbb{E}_{q_i} \left[\log \frac{q_i^{(k)}}{q_i^{(k)}(\mathbf{y})} \right] \\ & - \sum_{j \in \mathcal{N}_i} \frac{A_{ij}}{\alpha_k} \mathbb{E}_{q_i} [\log q_j^{(k)}(\mathbf{y})]. \end{aligned} \quad (29)$$

With the above objective, we can compute the derivatives with respect to $\boldsymbol{\mu}_i$ and Σ_i as follows

$$\begin{aligned} \frac{\partial g_i^{(k)}}{\partial \boldsymbol{\mu}_i^\top} = & \Sigma_i^{-1} \mathbb{E}_{q_i} [(\mathbf{s}_i - \boldsymbol{\mu}_i) \frac{\delta c_i}{\delta q_i}(q_i^{(k)})] \\ & - \frac{1}{\alpha_k} \Sigma_i^{-1} \mathbb{E}_{q_i} \left[(\mathbf{s}_i - \boldsymbol{\mu}_i) \log \frac{q_i^{(k)}}{q_i^{(k)}(\mathbf{y})} \right] \\ & - \sum_{j \in \mathcal{N}_i} \frac{A_{ij}}{\alpha_k} \Sigma_i^{-1} \mathbb{E}_{q_i} [(\mathbf{s}_i - \boldsymbol{\mu}_i) \log q_j^{(k)}(\mathbf{y})], \end{aligned} \quad (30)$$

$$\begin{aligned} \frac{\partial g_i^{(k)}}{\partial \boldsymbol{\mu}_i^\top \partial \boldsymbol{\mu}_i} = & \Sigma_i^{-1} \mathbb{E}_{q_i} [(\mathbf{s}_i - \boldsymbol{\mu}_i)(\mathbf{s}_i - \boldsymbol{\mu}_i)^\top \frac{\delta c_i}{\delta q_i}(q_i^{(k)})] \Sigma_i^{-1} \\ & - \frac{1}{\alpha_k} \Sigma_i^{-1} \mathbb{E}_{q_i} [(\mathbf{s}_i - \boldsymbol{\mu}_i)(\mathbf{s}_i - \boldsymbol{\mu}_i)^\top \log \frac{q_i^{(k)}}{q_i^{(k)}(\mathbf{y})}] \Sigma_i^{-1} \\ & - \sum_{j \in \mathcal{N}_i} \frac{A_{ij}}{\alpha_k} \Sigma_i^{-1} \mathbb{E}_{q_i} [(\mathbf{s}_i - \boldsymbol{\mu}_i)(\mathbf{s}_i - \boldsymbol{\mu}_i)^\top \log q_j^{(k)}(\mathbf{y})] \Sigma_i^{-1}, \end{aligned}$$

$$\begin{aligned} \frac{\partial g_i^{(k)}}{\partial \Sigma_i} = & \frac{1}{2} \Sigma_i^{-1} \mathbb{E}_{q_i} [(\mathbf{s}_i - \boldsymbol{\mu}_i)(\mathbf{s}_i - \boldsymbol{\mu}_i)^\top \frac{\delta c_i}{\delta q_i}(q_i^{(k)})] \Sigma_i^{-1} \\ & - \frac{1}{2\alpha_k} \left(\Sigma_i^{-1} + \Sigma_i^{-1} \mathbb{E}_{q_i} [(\mathbf{s}_i - \boldsymbol{\mu}_i)(\mathbf{s}_i - \boldsymbol{\mu}_i)^\top \log \frac{q_i^{(k)}}{q_i^{(k)}(\mathbf{y})}] \Sigma_i^{-1} \right) \\ & - \sum_{j \in \mathcal{N}_i} \frac{A_{ij}}{2\alpha_k} \Sigma_i^{-1} \mathbb{E}_{q_i} [(\mathbf{s}_i - \boldsymbol{\mu}_i)(\mathbf{s}_i - \boldsymbol{\mu}_i)^\top \log q_j^{(k)}(\mathbf{y})] \Sigma_i^{-1}. \end{aligned}$$

We can see that,

$$\frac{\partial g_i^{(k)}}{\partial \boldsymbol{\mu}_i^\top \partial \boldsymbol{\mu}_i} = 2 \frac{\partial g_i^{(k)}}{\partial \Sigma_i} + \frac{1}{\alpha_k} \Sigma_i^{-1} \quad (31)$$

To compute $\frac{\partial g_i^{(k)}}{\partial \boldsymbol{\mu}_i^\top \partial \boldsymbol{\mu}_i}$, following [34], we make use of *Stein's lemma* [46]:

$$\mathbb{E}_{q_i} [(\mathbf{s}_i - \boldsymbol{\mu}_i) f_i(\mathbf{s}_i)] \equiv \Sigma_i \mathbb{E}_{q_i} \left[\frac{\partial f_i(\mathbf{s}_i)}{\partial \mathbf{s}_i^\top} \right]. \quad (32)$$

Note that $\frac{\delta c_i}{\delta q_i}(q_i^{(k)})$, $\log q_i^{(k)}$ and $\log q_i^{(k)}(\mathbf{y})$ are all functions of \mathbf{s}_i . We have $\frac{\delta c_i}{\delta q_i} = -\log p_i(\mathbf{s}_i, \mathbf{z}_i, \mathbf{u}_i) + \log q_i(\mathbf{s}_i) + 1$ [47, Proposition 1] and $\log p_i(\mathbf{s}_i, \mathbf{z}_i, \mathbf{u}_i)$ can be decomposed with (3) so that (30) can be rewritten as

$$\begin{aligned} \frac{\partial g_i^{(k)}}{\partial \boldsymbol{\mu}_i^\top} = & \mathbb{E}_{q_i} \left[\frac{\partial \frac{\delta c_i}{\delta q_i}(q_i^{(k)})}{\partial \mathbf{s}_i^\top} \right] - \frac{1}{\alpha_k} \mathbb{E}_{q_i} \left[\frac{\partial \log q_i^{(k)}}{\partial \mathbf{s}_i^\top} \right] \\ & + \frac{1}{\alpha_k} \mathbb{E}_{q_i} \left[\frac{\partial \log q_i^{(k)}(\mathbf{y})}{\partial \mathbf{s}_i^\top} \right] - \sum_{j \in \mathcal{N}_i} \frac{A_{ij}}{\alpha_k} \mathbb{E}_{q_i} \left[\frac{\partial \log q_j^{(k)}(\mathbf{y})}{\partial \mathbf{s}_i^\top} \right] \\ = & -\bar{F}_i^{-\top} \bar{W}_i^{-1} (\bar{G}_i^\top \mathbf{u}_i - \bar{F}_i^{-1} \boldsymbol{\mu}_i) - \bar{H}_i^\top \bar{V}_i^{-1} (\mathbf{z}_i - \bar{H}_i \boldsymbol{\mu}_i) \\ & - \Sigma_{i,(k)}^{-1} (\boldsymbol{\mu}_i - \boldsymbol{\mu}_{i,(k)}) + \frac{1}{\alpha_k} \Sigma_{i,(k)}^{-1} (\boldsymbol{\mu}_i - \boldsymbol{\mu}_{i,(k)}) \\ & - \frac{1}{\alpha_k} L^\top \Sigma_{i,(k)}^{-1} L (\boldsymbol{\mu}_i - \boldsymbol{\mu}_{i,(k)}) \\ & + \frac{1}{\alpha_k} \sum_{j \in \mathcal{N}_i} A_{ij} L^\top \Sigma_{j,(k)}^{-1} L (\boldsymbol{\mu}_i - \boldsymbol{\mu}_{j,(k)}). \end{aligned} \quad (33)$$

where $\boldsymbol{\mu}_{i,(k)}$, $\Sigma_{i,(k)}$ are the mean and covariance for $q^{(k)}$ respectively and $L = [0 \ I]$ such that

$$L^\top \Sigma_i^{\mathbf{y}} L = \begin{bmatrix} 0 & 0 \\ 0 & \Sigma_i^{\mathbf{y}} \end{bmatrix}. \quad (34)$$

Therefore, the second derivative with respect to $\boldsymbol{\mu}_i$ is

$$\begin{aligned} \frac{\partial g_i^{(k)}}{\partial \boldsymbol{\mu}_i^\top \partial \boldsymbol{\mu}_i} &= \bar{F}_i^{-\top} \bar{W}_i^{-1} \bar{F}_i^{-1} + \bar{H}_i^\top \bar{V}_i^{-1} \bar{H}_i - \Sigma_{i,(k)}^{-1} \\ &+ \frac{1}{\alpha_k} (\Sigma_{i,(k)}^{-1} - L^\top \Sigma_{i,(k)}^{\mathbf{y}-1} L + \sum_{j \in \mathcal{N}_i} A_{ij} L^\top \Sigma_{j,(k)}^{\mathbf{y}-1} L). \end{aligned} \quad (35)$$

Setting $\frac{\partial g_i^{(k)}}{\partial \Sigma_i} = 0$ and using (31)(35), we get

$$\begin{aligned} \Sigma_i^{-1} &= \alpha_k (\bar{F}_i^{-\top} \bar{W}_i^{-1} \bar{F}_i^{-1} + \bar{H}_i^\top \bar{V}_i^{-1} \bar{H}_i - \Sigma_{i,(k)}^{-1}) \\ &+ \Sigma_{i,(k)}^{-1} - L^\top \Sigma_{i,(k)}^{\mathbf{y}-1} L + \sum_{j \in \mathcal{N}_i} A_{ij} L^\top \Sigma_{j,(k)}^{\mathbf{y}-1} L. \end{aligned} \quad (36)$$

Further setting $\frac{\partial g_i^{(k)}}{\partial \boldsymbol{\mu}_i} = 0$ and using (33)(36), we get

$$\begin{aligned} \Sigma_i^{-1} \boldsymbol{\mu}_i &= \alpha_k (\bar{F}_i^{-\top} \bar{W}_i^{-1} \bar{G}_i \mathbf{u}_i + \bar{H}_i^\top \bar{V}_i^{-1} \mathbf{z}_i - \Sigma_{i,(k)}^{-1} \boldsymbol{\mu}_{i,(k)}) \\ &+ \Sigma_{i,(k)}^{-1} \boldsymbol{\mu}_{i,(k)} - L^\top \Sigma_{i,(k)}^{\mathbf{y}-1} L \boldsymbol{\mu}_{i,(k)} + \sum_{j \in \mathcal{N}_i} A_{ij} L^\top \Sigma_{j,(k)}^{\mathbf{y}-1} L \boldsymbol{\mu}_{j,(k)}. \end{aligned} \quad (37)$$

Note that $\mathcal{G}(\Sigma_{i,(k)}^{\mathbf{y}-1} \boldsymbol{\mu}_{i,(k)}, \Sigma_{i,(k)}^{\mathbf{y}-1})$ is the marginal distribution in the information space. In this way

$$\sum_{j \in \mathcal{N}_i} A_{ij} L^\top \Sigma_{j,(k)}^{\mathbf{y}-1} L = \begin{bmatrix} 0 & 0 \\ 0 & \sum_{j \in \mathcal{N}_i} A_{ij} \Sigma_{j,(k)}^{\mathbf{y}-1} \end{bmatrix} = \begin{bmatrix} 0 & 0 \\ 0 & \bar{\Sigma}_{i,(k)}^{\mathbf{y}-1} \end{bmatrix}. \quad (38)$$

Similarly,

$$\begin{aligned} \sum_{j \in \mathcal{N}_i} A_{ij} L^\top \Sigma_{j,(k)}^{\mathbf{y}-1} L \boldsymbol{\mu}_{j,(k)} &= \begin{bmatrix} \mathbf{0} \\ \sum_{j \in \mathcal{N}_i} \Sigma_{j,(k)}^{\mathbf{y}-1} \boldsymbol{\mu}_{j,(k)} \end{bmatrix} \\ &= \begin{bmatrix} \mathbf{0} \\ \bar{\Sigma}_{i,(k)}^{\mathbf{y}-1} \bar{\boldsymbol{\mu}}_{i,(k)} \end{bmatrix}. \end{aligned} \quad (39)$$

Finally, setting

$$\begin{aligned} \bar{\Omega}_{i,(k)} &= \Sigma_{i,(k)}^{-1} - L^\top \Sigma_{i,(k)}^{\mathbf{y}-1} L + \sum_{j \in \mathcal{N}_i} A_{ij} L^\top \Sigma_{j,(k)}^{\mathbf{y}-1} L, \\ \bar{\omega}_{i,(k)} &= \Sigma_{i,(k)}^{-1} \boldsymbol{\mu}_{i,(k)} - L^\top \Sigma_{i,(k)}^{\mathbf{y}-1} L \boldsymbol{\mu}_{i,(k)} \\ &+ \sum_{j \in \mathcal{N}_i} A_{ij} L^\top \Sigma_{j,(k)}^{\mathbf{y}-1} L \boldsymbol{\mu}_{j,(k)}, \end{aligned} \quad (40)$$

we can verify that

$$\begin{aligned} \bar{\Omega}_{i,(k)}^{-1} &= \bar{\Sigma}_{i,(k)} = \begin{bmatrix} A \bar{\Sigma}_{i,(k)}^{\mathbf{y}} A^\top + P & A \bar{\Sigma}_{i,(k)}^{\mathbf{y}} \\ \Sigma_{i,(k)}^{\mathbf{y}} A^\top & \bar{\Sigma}_{i,(k)}^{\mathbf{y}} \end{bmatrix} \\ \bar{\Sigma}_{i,(k)} \bar{\omega}_{i,(k)} &= \bar{\boldsymbol{\mu}}_{i,(k)} = \begin{bmatrix} A \bar{\boldsymbol{\mu}}_{i,(k)}^{\mathbf{y}} + \mathbf{b} \\ \bar{\boldsymbol{\mu}}_{i,(k)}^{\mathbf{y}} \end{bmatrix}, \end{aligned} \quad (41)$$

where

$$\begin{aligned} A &= \Sigma_{i,(k)}^{\mathbf{x}\mathbf{y}} \Sigma_{i,(k)}^{\mathbf{y}-1}, \mathbf{b} = \boldsymbol{\mu}_{i,(k)}^{\mathbf{x}} - \Sigma_{i,(k)}^{\mathbf{x}\mathbf{y}} \Sigma_{i,(k)}^{\mathbf{y}-1} \boldsymbol{\mu}_{i,(k)}^{\mathbf{y}}, \\ P &= \Sigma_{i,(k)}^{\mathbf{x}} - \Sigma_{i,(k)}^{\mathbf{x}} \Sigma_{i,(k)}^{\mathbf{y}-1} \Sigma_{i,(k)}^{\mathbf{x}\mathbf{y}\top}. \end{aligned} \quad (42)$$

By substituting $\bar{\Omega}_{i,(k)} = \bar{\Sigma}_{i,(k)}^{-1}$ and $\bar{\omega}_{i,(k)} = \bar{\Sigma}_{i,(k)}^{-1} \bar{\boldsymbol{\mu}}_{i,(k)}$ into (40) and further into (36)(37), we will get exactly the same result as in Proposition 3 (16), thus completing the proof.

The result can also be interpreted by Proposition 1, (38) and (39) are geometric averaging of the marginal Gaussians over \mathbf{y} [48, Lemma 1] which correspond to $\prod_{j \in \mathcal{N}_i} [q_j^{(k)}(\mathbf{y})]^{A_{ij}}$ in (9). (41) is constructing a new joint distribution with the averaged marginal (Proposition 2) which correspond to $q_i^{(k)}(\mathbf{x}_i | \mathbf{y}) \prod_{j \in \mathcal{N}_i} [q_j^{(k)}(\mathbf{y})]^{A_{ij}}$ in (9). The step term $\alpha_k (\bar{F}_i^{-\top} \bar{W}_i^{-1} \bar{F}_i^{-1} + \bar{H}_i^\top \bar{V}_i^{-1} \bar{H}_i - \Sigma_{i,(k)}^{-1})$ and $\alpha_k (\bar{F}_i^{-\top} \bar{W}_i^{-1} \bar{G}_i \mathbf{u}_i + \bar{H}_i^\top \bar{V}_i^{-1} \mathbf{z}_i - \Sigma_{i,(k)}^{-1} \boldsymbol{\mu}_{i,(k)})$ correspond to $[p_i(\mathbf{x}_i, \mathbf{y}, \mathbf{z}_i, \mathbf{u}_i) / q_i^{(k)}(\mathbf{x}_i, \mathbf{y})]^{\alpha_k}$ in (9).